PAPER

Check for updates

Reverse water gas shift reaction over a Cu/ZnO catalyst supported on regenerated spent bleaching earth (RSBE) in a slurry reactor: the effect of the Cu/Zn ratio on the catalytic activity

Melissa Low Phey Phey,[ab] Tuan Amran Tuan Abdullah,*[ab] Umi Fazara Md Ali,[cd] Mohamed Yusuf Mohamud, [iD][ab] Muhammad Ikram [iD]*[e] and Walid Nabgan [iD]*[f]

The catalytic conversion of CO_2 *via* the Reverse Water Gas Shift (RWGS) reaction for CO production is a promising environment-friendly approach. The greenhouse gas emissions from burning fossil fuels can be used to produce valuable fuels or chemicals through CO_2 hydrogenation. Therefore, this project was to study the CO_2 conversion *via* RWGS over various Cu/ZnO catalysts supported by regenerated spent bleaching earth (RSBE) prepared by wet impregnation technique with different Cu : Zn ratios (0.5, 1.0, 1.5, 2.0, 3.0). The causes of environmental pollution from the disposal of spent bleaching earth (SBE) from an edible oil refinery can be eliminated by using it as catalyst support after the regeneration process. The synthesized catalysts were characterized by thermogravimetric analysis (TGA), X-ray diffraction (XRD), temperature-programmed reduction of hydrogen ($TPR-H_2$), pyridine-adsorbed Fourier transform infrared (FTIR-pyridine), temperature programmed desorption of carbon dioxide ($TPD-CO_2$), N_2 physisorption, and Fourier transform infrared (FTIR) analysis. The RWGS reaction was carried out in a slurry reactor at 200 °C, with a pressure of 3 MPa, a residence time of 4 h, and catalyst loading of 1.0 g with an H_2/CO_2 ratio of 3. According to experimental data, the Cu/Zn ratio significantly impacts the catalytic structure and performance. The catalytic activity increased until the Cu : Zn ratio reached the maximum value of 1.5, while a further increase in Cu/Zn ratio inhibited the catalytic performance. The CZR3 catalyst (Cu/Zn ratio of 1.5) with a higher catalytic reducibility, high copper dispersion with small crystalline size, lower total pore volume as well as higher basicity showed superior catalytic performance in terms of CO_2 conversion (40.67%) and CO yield (39.91%). Findings on the effect of reaction conditions revealed that higher temperature (>240 °C), higher pressure (>3 MPa), higher reaction time (>4 h) and higher catalyst loading (>1.25 g) could improve CO_2 conversion to CO yield. A maximum CO_2 conversion of 45.8% and multiple recycling stability of the catalyst were achieved, showing no significant decrease in CO_2 conversion.

1. Introduction

The accumulation of ambient greenhouse gases (GHG) has reached an unprecedented level, primarily resulting in global warming, and is known to be a significant anthropogenic source. The main GHG is carbon dioxide (CO_2), which has acted as the driving force of global warming and climate change in recent years. CO_2 concentrations have been rising since the pre-industrial era, primarily due to fossil fuels like natural gas, petroleum and coal that people burn for energy, causing the depletion of fossil fuels and amplifying the earth's natural greenhouse effect. Recent evidence by the State of the Climate in 2020 report from the American Meteorological Society (AMS) and the National Oceanic and Atmospheric Administration (NOAA) reports that the global atmospheric concentration of CO_2 reached 412.5 ppm in the year 2020, achieving a new high record.[1] In order to monitor the rise in the average global temperature by 2–3 °C, the global emission of CO_2 should be lowered by 50–80 per cent by 2050.[2] Rising CO_2 emission leads to global warming and climate change, causing a series of

[a]*Center of Hydrogen Energy, Institute of Future Energy, Universiti Teknologi Malaysia, 81310 Skudai, Johor, Malaysia. E-mail: tuanamran@utm.my*

[b]*Faculty of Chemical and Energy Engineering, Universiti Teknologi Malaysia, 81310, Skudai, Johor, Malaysia*

[c]*Chemical Engineering Programme, Faculty of Chemical Engineering Technology, Universiti Malaysia Perlis, Kompleks Pusat Pengajian Jejawi 3, 02600 Arau, Perlis, Malaysia*

[d]*Centre of Excellence Biomass Utilization (COEBU), Universiti Malaysia Perlis, Kompleks Pusat Pengajian Jejawi 3, 02600 Arau, Perlis, Malaysia*

[e]*Solar Cell Applications Research Lab, Department of Physics, Government College University Lahore, 54000, Punjab, Pakistan. E-mail: dr.muhammadikram@gcu.edu.pk*

[f]*Departament d'Enginyeria Química, Universitat Rovira i Virgili, Av Països Catalans 26, 43007, Tarragona, Spain. E-mail: walid.nabgan@urv.cat*

potential impacts on ecological, physical and health, including severe weather events such as storms, droughts, floods, heatwaves, the rise of the sea level, disrupted water systems, and altered crop growth.[3]

Due to the irreversible consumption of existing energy supply and finite, and non-renewable fossil fuels in the world, the exploitation of alternative energy sources to replace conventional fossil fuels is vital. As CO_2 is relatively abundant, globally distributed, available, and affordable, utilization of CO_2 improves the security and stability of the energy system. Furthermore, the utilization of CO_2 is considered with a lot of interest because it can recycle carbon, hence reducing the emission of CO_2. Therefore, it is crucial to develop research on the utilization and conversion of CO_2 into valuable products for managing carbon and sustainable development. Various technical methods, including catalytic, electrochemical, biological, photocatalytic, and photosynthetic processes, can turn CO_2 into commercial products.[4–9]

Due to the low rates of photoelectrochemical reduction, it is currently not practical to convert large amounts of CO_2 because it would be extremely challenging to scale up the process to match CO_2 production rates.[10,11] Similarly, using biomass will not allow for long-term storage of CO_2; instead, it will only allow for a reduction in atmospheric CO_2 concentrations if the biomass is converted to fuels. Furthermore, microalgae would probably be used in the CO_2 conversion processes with biomass that do not compete with food sources and do not require land. However, the costs associated with developing and maintaining these systems must be significantly reduced before it is practical.[12,13] For thermochemical CO_2 splitting, a metal oxide with high oxygen mobility has oxygen vacancies that allow the reduction of CO_2 to CO. This approach has been used to reduce a variety of oxides, but they often need to be reduced for several hours at lower temperatures or at least 1000 °C to generate oxygen vacancies.[14–18] As a result of the high operating temperatures, specialist gear and supplementary machinery, such as solar concentrators that can produce heat input, are required.

Conversely, reverse water gas shift (RWGS) reaction can be implemented due to the numerous local benefits associated with renewable electricity sources, which can help create a closed carbon loop. Generating hydrogen using electrolysis has far lower startup costs than employing solar thermal heating to increase the low-intensity solar flux to practical levels. Additionally, a very flexible chemical intermediate can be produced by the RWGS reaction. Instead, photocatalysis's main hydrocarbon methane product still needs to be processed before use. The RWGS reaction could be helpful in situations where H_2 is readily available, like space exploration, where electrolysis is predominantly utilized to create synthetic air.[19] Its use in upcoming CO_2 conversion techniques seems likely a result of these factors and the readiness of the rWGS processes.

Many gas-phase catalytic processes involving solid catalysts have been explored in this field. For instance, RWGS reaction, methanol synthesis and methanation have all been the topic of extensive catalysis studies. However, the RWGS reaction has been hailed as a practical method for arbitrary control of the

$H_2 : CO$ composition ratio in synthesis gas which is in great demand as a raw material for C1 chemistry.[20] Transformation of CO_2 to carbon monoxide (CO) and water utilizing hydrogen in a catalytic reverse water gas shift (RWGS) reaction (eqn (1)) has been perceived as one of the most promising methods for CO_2 usage technologies, which has been the subject of various investigations.[21–28]

$$CO_2 + H_2 \leftrightarrow CO + H_2O \ \Delta H_{298K}^0 = +41 \text{ kJ mol}^{-1} \quad (1)$$
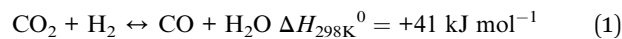
CO_2 is generally less reactive due to its chemical stability, so converting it to more receptive CO requires a lot of energy.[23] RWGS reaction is endothermic and prefers higher temperatures to accomplish satisfactory degrees of activity, following Le Châtelier's principle. Furthermore, lower pressure input also supposes a considerable advantage for RWGS reaction.[29] Nonetheless, this pressure and temperature are restricted to guarantee that the conditions used during the experimental phases are monetarily gainful for commercial applications. The biggest advantages of the RWGS reaction is the resulting CO can be further converted to valuable chemicals such as dimethyl ether, methanol and long-chain hydrocarbons, using well-developed synthesis gas (CO and H_2) transformation innovations like Fischer–Tropsch (FT) synthesis and methanol synthesis.[21,23,30,31] These techniques make the RWGS reaction an appealing platform for using CO_2 as a C_1 building block in chemical construction to produce demanded commodities.

The high-pressure RWGS reaction has several drawbacks, including the costlier materials required for the reactor, higher risk of carbon formation and methane generation. Due to the endothermic character, CO is produced from CO_2 at greater temperatures up to 800 °C. Therefore, adding the hydrogen-rich feedstock or increasing the reaction temperature is required to achieve excellent results. The high temperatures could shorten the life of the catalyst and reactor by encouraging undesirable occurrences.[32] Reduced temperature ranges would help to reduce the process energy and capital costs. Due to the low equilibrium constant, driving the RWGS to completion at lower reaction temperatures would be challenging. However, increasing the H_2 concentration can move the equilibrium to the right by forcing CO_2 consumption.[32] Fewer endeavors have been made towards advancing dynamic and stable catalysts for the RWGS reaction that can operate at low temperatures with enhanced CO_2 conversion and CO production. RWGS catalysts are being investigated to create an industrially viable carbon recycling route.

Over the past few decades, various catalysts for RWGS have been studied, explored and published in the literature.[30] Several metal-based catalysts have been employed to generate carbon monoxide (Pt, Pd, Rh, Ru, Au, Fe, Mo, Cu, Co, Ni). Still, the Cu catalyst is one of the most investigated systems because of its relatively low cost, high activity and selectivity.[21] Cu can be operated at a low-temperature range (~165 °C) and produce near zero methane as a side product, which is regularly respected to be effective due to its enhanced adsorption of reaction intermediates at lower temperatures.[33–35] However, the feasibility of Cu systems is limited by deactivation issues with

metal sintering caused by the high operating temperatures. Therefore, the addition of Zn acts as a stabilizer and dispersant. Still, since the interface interaction is associated with the copper phase, it has additionally been accounted for as supplying active centers and causing synergetic impacts.[36–38] For Cu/ZnO-based catalysts, different Cu : Zn ratios are the primary determinants in the catalytic activity of CO_2/H_2 reactions. The conversion of CO_2 has been closely related to the theoretical concentration of Cu–ZnO contacts. Though, the active sites where CO is formed are thought to differ. In addition, support can also be added to the Cu/ZnO catalyst system to boost its stability and activity.

Spent bleaching earth (SBE), also known as spent clay, is a type of solid waste that is produced during the pretreatment of crude palm oil (CPO) in an edible oil refinery from the process of treating and removing the dyes and poisons from raw oil.[39–42] SBE is an aluminosilicate mineral that mainly comprises montmorillonites with a 2 : 1 unit layer structure.[43] Montmorillonite is increasingly used as a catalyst or catalyst support in many organic reactions.[44] The worldwide SBE waste production is estimated at 600 000 tonnes.[42] Malaysia, the world's second-largest producer of crude palm oil, produces more than 100 000 tonnes of SBE annually.[45] Depending on the bleaching activity, SBE often carries 20 to 40% residual oil by weight.[40,46] However, due to the autocatalytic action of clay minerals and the correlation of GHG emissions upon the disposal of SBE, the oxidation of residual oil in the earth to the point of spontaneous auto-ignition will result in fire and pollution problems.[39–41,47] Therefore, rather than being disposed of and contributing to the pollution, this study proposes the regenerated spent blenching earth (RSBE), which will be used as the supported catalyst due to the main component of SBE is SiO_2 (~48%), followed by Al_2O_3 (~20%), CaO (~12%), MgO (4.7) and SO_3 (3.2%).[48] The great potential for silica and alumina sources is high in the surface area making SBE suitable to act as catalyst support after the regeneration process.

This work evaluates the performance of Cu/ZnO catalysts supported on high-surface RSBE. To our knowledge, the effects of varied Cu/Zn ratios supported on RSBE for RWGS catalytic performance have not been reported. Along these lines, a detailed analysis was done of how the physicochemical characteristics of the catalysts affected the RWGS reaction. Additionally, several characterization approaches were employed to learn more about the relationship between chemical properties and catalysis. Besides, there is a scarcity of information on the RWGS reaction operating in a slurry reactor at low temperatures and elevated pressure conditions. Finally, the stability of the most promising catalyst over five reaction cycles could be demonstrated in the slurry phase application. The impressive catalytic improvements achieved by Cu/ZnO catalysts supported on RSBE indicate a significant advancement in the design of highly active yet reasonably priced RWGS catalysts. From a technical point of view, keeping the reaction temperature as low as possible is suggested to save money and energy.

2. Experimental methods

2.1. Materials

Spent bleaching earth (SBE) was obtained from a palm oil refinery (Sime Darby Sdn. Bhd), Pasir Gudang, Johor, Malaysia. Copper(II) nitrate trihydrate ($CuN_2O_63H_2O$, ≥99% purity), zinc nitrate hexahydrate ($ZnN_2O_66H_2O$, ≥99.0% purity) and light mineral oil were purchased from Sigma-Aldrich, Malaysia. The nitric acid (HNO_3) was purchased from RCl Labscan.

2.2. Regeneration process of SBE

SBE was calcined in the air atmosphere at 500 °C for 3 h, followed by mild acid treatment (1 M of nitric acid). The SBE and nitric acid (w/v) ratio used in the acid treatment procedure was 1 : 5. Nitric acid and SBE were mixed, and the mixture was stirred at 80 °C for 2 h using a magnetic stirrer. Then, SBE was filtered and repeatedly rinsed with distilled water until the pH level reached 7 to remove the acid. The RSBE was dried for 24 h at 105 °C before being employed as support in the Cu/ZnO-based catalyst for the RWGS experiment.

2.3. Catalyst preparation

The chemicals used for catalyst preparation for methanol synthesis are copper nitrate trihydrate ($CuN_2O_63H_2O$) and zinc nitrate hexahydrate ($ZnN_2O_66H_2O$). 5 different weight percentages of Cu/Zn composition catalyst supported on RSBE were synthesized by wet impregnation method. 15 wt% of the active component was supported on 85 wt% of RSBE. Table 1 shows the composition of the catalysts studied. From Table 1, Cu (wt%) and Zn (wt%) represent the mass fraction of the atoms. At first, 150 mL of copper nitrate trihydrate and zinc nitrate hexahydrate solution were impregnated on 8.5 g of RSBE. The solution was mixed entirely using the magnetic force stirrer with heat at 80 °C for 4 h. The slurry catalyst was dried for 24 h at 105 °C in an oven. After the calcination stage of catalysts in the air atmosphere at 400 °C for 3 h, the catalysts were allowed to cool down to room temperature in a desiccator to prevent exposure to moisture.

2.4. Characterization methods

Shimadzu TGA-50 was used to identify optimum calcination temperature and thermal stability for prior calcined catalysts. Air was supplied on prior-calcined catalysts to evolved gases. Approximately 10–12 mg of each catalyst was loaded into an alumina sample cell of the analyzer. After that, each catalyst was heated in situ with continuous air flow (20 mL min^{-1}) at a rate of

Table 1 Weight percentage of each catalyst's composition

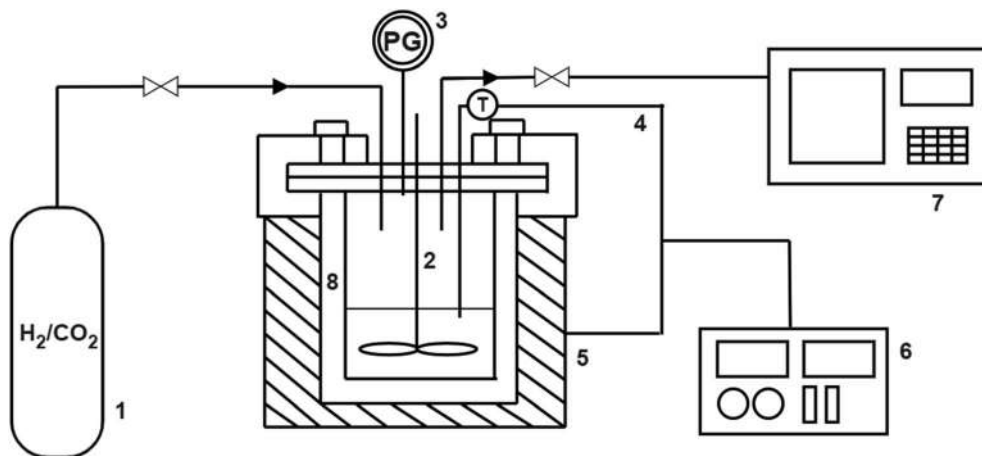| Catalyst symbol	Cu/Zn ratio	Cu (wt%)	Zn (wt%)	RSBE (wt%)
CZR1	0.5	5	10	85
CZR2	1.0	7.5	7.5	85
CZR3	1.5	9	6	85
CZR4	2.0	10	5	85
CZR5	3.0	11.25	3.75	85
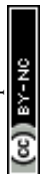
Fig. 1 Schematic diagram of CO_2 hydrogenation experimental setup: (1) H_2/CO_2 tank; (2) stirrer; (3) pressure gauge; (4) thermocouple; (5) heater; (6) temperature and motor controller; (7) GC; (8) reactor.

10 °C min^{-1}. The catalysts' exothermic weight loss was determined over a temperature range of 30–800 °C.

Temperature-programmed reduction of hydrogen (TPR-H_2) analysis was performed to examine the reduction behaviour of the catalyst on the support. TPR-H_2 experiments were carried out in a chemisorption analyzer, Micromeritics Chemisorb 2720 equipped with a thermal conductivity detector (TCD). To ensure the catalyst's surface is free of moisture and contaminants, 50 mg of the catalyst was heated in a U-shape reactor at 300 °C for 30 min in a helium stream (purity 99.99%) at 30 mL min^{-1}. After the sample was cooled to room temperature, the catalyst was heated with 10% H_2/Ar mixture flowing continuously with gas volume velocity at 30 mL min^{-1} in the temperature range of 25–800 °C. TPR-H_2 profile was collected at a linearly programmed rate of 20 °C min^{-1} under atmospheric pressure. The H_2 consumption was monitored by recording the TCD signal in increasing the sample temperature.

X-ray diffraction (XRD) experiment was carried out on an X-ray diffractometer (Smart Lab, Rigaku, Japan) with a Cu target Kα radiation at 40 kV and 30 mA in the scanning range of $2\theta =$ 10 to 80° at a scanning speed of 2° per min to determine the crystallite size of the reduced catalysts.

FTIR measurements were carried out on an Agilent Cary 640 FTIR spectrometer equipped with a high-temperature stainless steel cell with CaF_2 windows. All samples had a 1 h pretreatment at 400 °C. The basic probe molecule pyridine was employed to assess the catalyst's acidity. The activated catalyst was exposed to 2 Torr of pyridine at 150 °C for 15 min to assess pyridine adsorption.

Temperature programmed desorption of carbon dioxide (TPD-CO_2) experimental tests were investigated in the identical appliances TPR-H_2 employing at the TCD to evaluate the basicity property of the catalyst surface. First, 50 mg of the reduced catalyst was purged in a pure helium (99.99%) stream at 30 mL min^{-1} and temperature of 200 °C for 1 h to eliminate the absorbed humidity, impurities and gases. The catalyst was exposed to CO_2 at 50 °C for 1 h at 30 mL min^{-1} after cooling to ambient temperature, and physisorbed molecules were then

removed by adsorption in the helium stream for 30 min. The catalyst was flushed with helium flow at 30 mL min^{-1} to evacuate the physical adsorbed CO_2 from 50 to 900 °C at 20 °C min^{-1} of heating rate.

The total surface area and porosity of the prepared catalysts and support materials were determined using a surface area and porosity analyzer (Micromeritics TriStar II) *via* nitrogen (N_2) adsorption–desorption isotherms at 77 K over a relative pressure (p/p_0). Before analysis, the reduced catalysts were degassed under vacuum for 24 h at 150 °C to eliminate any adsorbed gas and contaminants that have been adsorbing on the catalyst surface. The BET surface area (S_{BET}) was determined using the BET method within the relative pressure range from 0.05 to 0.30 using 0.162 nm^2 as the N_2 molecule cross-sectional area. The total pore volume (V_{total}) was determined using Barrett–Joyner–Halenda (BJH) method from the desorption isotherm branch of the N_2 isotherm at the highest p/p_0 of 0.99.

Fourier transform infrared (FTIR) spectra were obtained over 400–4000 cm^{-1} using a SHIMADZU IRPrestige-21 IRAffinity-1 FTIR-8400S to identify the functional groups on the ready catalyst and RSBE support structure. The difference spectrum was created by subtracting a KBr backdrop from the sample scan.

High-resolution transmission electron microscopy (HRTEM) images were acquired with a JEOL JEM-ARM200F transmission electron microscope (TEM) operated at 200 kV. The sample was deposited onto a copper grid coated with a thin holey carbon film and dried in a vacuum overnight at room temperature.

2.5. Catalytic activity tests

The RWGS experiments were performed in a 100 mL slurry stirrer reactor, Parr reactor Series 4560. Fig. 1 shows the experimental setup of the RWGS reaction. Prior to each test, the calcined catalyst was reduced at 350 °C in H_2 flow with 20 mL min^{-1} for 3 h. All the experiments were carried out with 25 mL of light mineral oil as a reaction medium. A slurry made of 1.0 g of the reduced catalyst and light mineral oil was used for

the catalyst testing. The reactor was purged with reactant gases (H_2/CO_2) to remove any air and other gases. After purging, the H_2/CO_2 was fed into the reactor at a ratio of 3. The reactor was adjusted to 200 °C and pressurized to 3 MPa. The experiment was maintained constant for the entire run (4 h). The reactor was adjusted to 800 rpm for gas entrainment during the reaction. Gas samples were measured using Hewlett Packard 5890 Series II gas chromatography equipped capillary column HP-Plot Q with a thermal conductivity detector (TCD) and flame ionization detector (FID). The influence of the Cu/Zn molar ratio on CO_2 conversion and CO yield were investigated in fixed reaction parameters. The study began with the catalyst screening and was followed by the parametric study of the most promising catalyst to investigate the effect of operating parameters on RWGS performance. The effect of temperature (180–280 °C), pressure (1–5 MPa), reaction time (1–6 h), and catalyst loading (0.25–1.50 g) on CO_2 conversion and CO yield was investigated in the slurry system. Finally, the stability of the most promising catalyst with optimum operating parameters could be demonstrated in the slurry phase application over five reaction cycles.

In this study, the CO_2 conversion, X_{CO_2}, CO yield, Y_{CO} and H_2O yield was calculated based on the internal standardization method as the following formula:

$$X_{CO_2}(\%) = \frac{\text{mol of } CO_{2\text{ input}} - \text{mol of } CO_{2\text{ output}}}{\text{mol of } CO_{2\text{ input}}} \times 100 \quad (2)$$

$$Y_{CO}(\%) = \frac{\text{mol of } CO_{\text{output}}}{\text{mol of } CO_{2\text{ input}}} \times 100 \quad (3)$$

$$Y_{H_2O}(\%) = \frac{\text{mol of } H_2O_{\text{output}}}{\text{mol of } CO_{2\text{ input}}} \times 100 \quad (4)$$

3. Results and discussions

3.1. Catalyst characterization

3.1.1. TGA analysis. Thermogravimetric analysis (TGA) was performed in synthetic air to investigate the optimum calcination temperature and thermal behaviour of prior-calcined catalysts ranging from room temperature to 800 °C. The TGA curves for all the prior-calcined catalysts are shown in Fig. 2. As observed in Fig. 2, the initial weight loss occurred between room temperature and 250 °C in both catalysts. This is explained by the thermal dehydration of water molecules trapped on the material's surface and the decomposition of volatile contaminants throughout the synthesis process. The decomposition of copper precursor to copper oxide (CuO) may have caused the second weight loss over 250 °C and further thermal decomposition of zinc precursor to zinc oxide (ZnO). During the catalyst preparation, the deposition of nitrate anions, copper, and zinc salts occurs, increasing the solid's weight. This weight loss is assigned to the decomposition of copper hydroxynitrate ($Cu_2NO_3(OH)_3$) and zinc hydroxynitrate ($Zn_5(NO_3)_2(OH)_8 \cdot 2H_2O$) structure under the thermal effect.[49–51] Besides, nitrate anions on the sample were decomposed into nitrogen dioxide (NO_2)
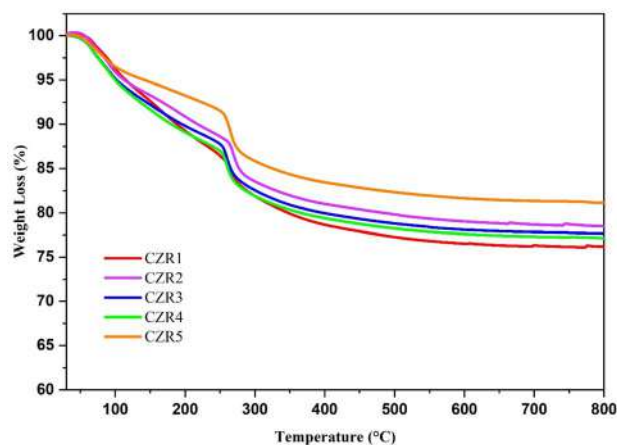

Fig. 2 TGA profile of prior-calcined catalysts.

and oxygen. The CuO and ZnO network is formed by the nitrate decomposition of oxygen atoms from $(NO_3)_2$ of copper and zinc salts. Fig. 2 shows the zero weight changes noticed above 600 °C, providing that the catalyst has finished decomposing.

However, more intensive sintering and recrystallization of copper, which results in a decrease in dispersion and catalytic activity, are side effects of high-temperature calcination on Cu/ZnO/Al$_2$O$_3$, claimed Kowalik & Próchniak (2010).[52] They demonstrated that reduced copper is constant at calcination temperatures above 380 °C. According to the study by Zhang *et al.* (2010), calcination affects the catalyst's CuO structure and the decomposition of the precursor.[53] Guo *et al.* (2011) found that the catalyst calcined at 400 °C achieved the highest activity.[54] The average CuO crystallite size increases as the calcination temperature increases, while the dispersion of Cu species reduces under the same conditions. Typically, calcination temperatures between 300 and 400 °C are ideal for producing a good catalyst.[55] So, the catalysts were calcined at the recommended calcination temperature of 400 °C to ensure the complete copper oxide phase development and stabilize the catalyst's mechanical characteristics (structure and textual). Besides, the calcination at 400 °C enabled all the decomposition of nitrate and copper salts and the dehydration reactions.

3.1.2. Temperature programme reduction of hydrogen (TPR-H_2) analysis. The reduction behaviour of the calcined catalysts and catalytic support, RSBE was determined using TPR-H_2 measurements. The results are presented in Fig. 2. In the temperature range of 100–800 °C, two reduction peaks for the catalysts were identified based on the degrees of reducibility of the metal–support interaction. It is noteworthy to observe that there is a reduction of metal oxide in catalyst support, RSBE.

Based on the reduction profile, the H_2 consumption at a low temperature ranging from 250 to 500 °C shows two classes of adsorption peaks, which correspond to the reduction of copper oxide to metallic copper (CuO + H_2 → Cu + H_2O) and the reduction of the metal oxide in RSBE support. There is only one peak for the reduction process of Cu species, showing that the precursor contained only one kind of CuO. In the reduction
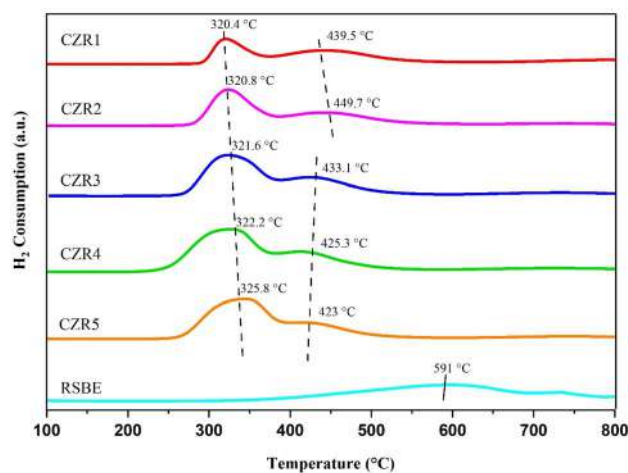
Fig. 3 H$_2$-TPR profiles of the calcined catalysts.

process, the CuO is directly reduced to copper, as demonstrated by the symmetry of the reduction peak. These findings suggest that all Cu species can be reduced to Cu^0 (Cu^{2+} → Cu^0) to produce a direct contact Cu–ZnO interface on RSBE support. Tasfy *et al.* (2017) reported on the impact of the Cu : ZnO ratio on SBA-15 in CO$_2$ hydrogenation and suggested that for low Cu content, just one reduction peak was identified, representing highly dispersed CuO.[56] Most of the CuO was reduced to metallic copper during hydrogen treatment, as seen by the diffraction peaks in the XRD patterns of reduced catalysts.

Interestingly, one peak appeared following the reduction of Cu species at a temperature from 420 to 450 °C. It is related to the reduction of transition metal oxides in the RSBE, as seen by the TPR profile of RSBE. Due to Cu insertions in the contacts between the support RSBE and active metal CuO, the second peak in both five catalysts could be less significant as compared to the reduction behaviour of RSBE alone. According to Thyssen, Maia, & Assaf (2015), copper has the property of lowering the reduction temperature of another metal due to the synergistic interaction between the metal oxide phases.[57] As a result, the decrease in the H$_2$ consumption of the RSBE in the catalysts can be explained (Fig. 3, 591 °C to 420–450 °C).[58]

The reduction peak gradually shifted to a higher temperature as the Cu/Zn ratio was increased from 0.5 to 3. According to the findings of Millar *et al.* (1998), this situation implies that a higher concentration of larger-sized copper oxide particles was created. The height and width of the peak increased with the increase of the Cu/Zn ratio for the catalyst, as seen in Fig. 3. This is in line with the findings of Ezeh *et al.*, who found that when ZnO content increased, the amount of easily reducible well-dispersed CuO increased as well.[59] Gesmanee *et al.* concluded that the increase of Zn metal amount in the system causes the reduction peak of Cu^{2+} to decrease.[60]

The altering of the catalyst system composition has only a little impact on the shape of the TPR profile. At lower temperatures, incomplete reduction of CuO to metallic Cu occurs, but metallic Cu agglomeration causes the catalyst to deactivate at higher temperatures. As a result, determining the

best and most appropriate reduction temperature is critical. The optimal reduction temperature for each catalyst changes depending on the interaction of the catalysts' compositions. In terms of the reduction temperature, many researchers feel that the lower the reduction temperature, the smaller the CuO particles should be.[61–63] The contribution of the first peak to the TPR pattern increased in the order: of CZR1 < CZR2 < CZR3 < CZR4 < CZR5. As a result, the reduction temperature of 350 °C was selected for both catalysts in this study.

The reducibility of CuO species increases in the following order: CZR1 < CZR2 < CZR3 < CZR4 < CZR5, which suggests that the interaction between CuO and ZnO on RSBE catalyst support in the CZR5 catalyst was more substantial than others. Fig. 2 indicates that the reduced peak temperature of the RSBE-supported catalysts shifts to a higher temperature, indicating a stronger metal–support interaction exists in the RSBE-supported catalysts. Therefore, the stronger interaction between CuO–ZnO and support reduced the risk of metal from agglomeration and sintering during the RWGS process.

3.1.3. XRD analysis. The crystallographic nature of the catalysts after reduction was characterized by XRD in the wide-angle region of 10° < 2θ < 80°, as illustrated in Fig. 4. All the catalysts showed low-intensity peaks attributable to CuO at 2θ of 39.4°, whereas extremely intense diffraction peaks related to metallic Cu at 2θ of 43.3°, 50.1° and 74.0°. It is attributed to the metallic Cu phase detected in all the reduced catalysts. It shows that every catalyst is activated by converting CuO to metallic Cu during the reduction process, regarded as the primary active phase in the RWGS reaction. On the other hand, the small amount of CuO diffraction peaks demonstrated that all CuO species are almost completely reduced throughout the reduction process. The low-intensity diffraction peak associated with ZnO is detected at 2θ = 36.5° in all the catalysts, demonstrating the direct contact Cu–ZnO interface on RSBE support produced after the reduction in H$_2$.[26] The diffraction peaks of Cu noticeably get stronger and sharper as the Cu/Zn ratio increases. In addition, the diffraction peaks of SiO$_2$ are detected at 2θ values
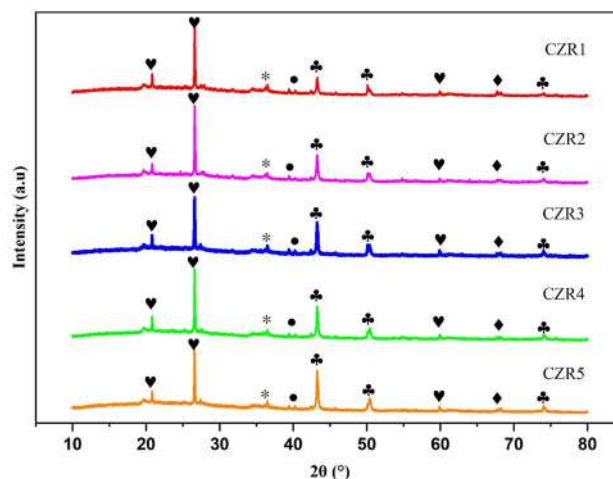

Fig. 4 XRD diffraction patterns of reduced catalysts. Crystalline phases: Cu (♣); CuO (●); ZnO (*); SiO$_2$ (♥); Al$_2$O$_3$ (◆).

Table 2 Metallic and textural properties of reduced catalysts

Catalyst	Cu crystallite size (nm)	Cu dispersion (%)	BET surface area ($m^2 g^{-1}$)	Total pore volume ($cm^2 g^{-1}$)	Average pore size (nm)
CZR1	26.71	3.78	59.56	0.2161	13.07
CZR2	26.79	3.77	68.73	0.2266	12.29
CZR3	27.10	3.73	66.76	0.2262	12.71
CZR4	28.20	3.58	70.08	0.2297	12.36
CZR5	30.44	3.32	99.49	0.2437	10.06
RSBE	—	—	196.20	0.2968	9.13

of 20.8°, 40.2° and 59.9°,[64] whereas Al_2O_3 is detected at 68.2°. The highest diffraction peaks observed in Fig. 4 at the 2θ value of 27.4° are attributed to the presence of quartz. Quartz is a crystalline mineral composed of SiO_2. The FTIR spectra corroborate the quartz present in the RSBE support. SiO_2 and Al_2O_3 are attributed to the main component, aluminosilicate of the bleaching earth, which contains in the RSBE support. The XRD spectra confirm that the phase distribution of RSBE remained after the regeneration process of SBE.

Cu dispersion and crystalline size are important factors in optimizing the interaction between Cu–ZnO and RSBE.[65] Cu has a crystal size band at 43.3°, as seen in Fig. 4, which is indexed as (111) plane of face-centred-cubic Cu metal, signifying the maximum dispersion of the Cu domains. Table 2 shows the crystal size of Cu particles and Cu dispersion, as calculated using the Scherrer equation, increases from 26.71 nm for CZR1 to 30.44 nm for CZR5 and decreases from 3.78% for CZR1 to 3.32% for CZR5, respectively (see Table 2). The presence of Zn promotes the dispersion of Cu species, which enhances the dissociation of the hydrogen molecules in the copper phase.[59,66] Ren et al. observed a similar trend and found that increased precursor concentration decreases Cu dispersion.[65]

The spectrum signal of the CZR1 catalyst was the least intense and had the largest full width at half maximum among other catalysts, implying that the CZR1 catalyst had the smallest Cu crystallite size (26.71 nm) and highest metal dispersion (3.78%). The presence of tiny Cu particles improved the exposed

surface area of the catalyst's active sites, resulting in the improvement of the catalytic activity.

3.1.4. Pyridine-adsorbed Fourier transform infrared (FTIR-pyridine) analysis. FTIR-pyridine analyses were performed to assess the acidity of the reduced catalysts. Fig. 5 shows the IR spectra of the pyridine adsorbed on the reduced catalysts at 150 °C. In general, the amount of pyridine adsorbed emphasizes the acidic surface character of the catalysts. It was observed that pyridine adsorbed on Lewis acid sites for both catalysts at 1448 cm^{-1}, while no peak emerged around wavelength 1540 cm^{-1}, which was attributed to pyridinium ions adsorbed on Brønsted acid sites. Because of the above statement, all the catalysts revealed strong interaction of pyridine with acidic sites at 150 °C, significantly exhibiting strong Lewis acid sites. A high intensity suggests that the catalyst has a lot of acid sites.

The band at 1448 cm^{-1} was slightly increased with the Cu : Zn ratio from 0.5 to 1.0. Adding the Cu/Zn ratio from 1.0 to 1.5 has caused a slight decrease in the acidic site, exhibiting a relatively stronger basicity of CZR3. The stronger band are observed on CZR4 and CZR5, which indicate that a larger amount of pyridine adsorbed on the catalysts. At the same time, their concentration is increased obviously, presenting the higher Cu/Zn ratio may be able to modify the acidic sites on the catalyst surface. The lowest concentration of the acidic site is shown on CZR3 (Cu/Zn ratio of 1.5).

The number of catalyst's acid increased in the following order: CZR3 < CZR1 < CZR2 < CZR4 < CZR5. It is noticeable that CZR3 had less accessible sites for pyridine adsorption compared to the other catalysts. This result demonstrated that fewer pyridine adsorption sites led to increased CO_2 adsorption on CZR3. However, the larger pyridine adsorption sites shown at CZR4 and CZR5 would prevent CO_2 from adsorbing or activating. These results were highly customized based on the basicity findings from the TPD-CO_2 analysis. These adjustments benefited the adsorption/activation of acidic gas CO_2 and further RWGS reaction to CO. Consequently, the Brønsted and Lewis acid sites on the surface of catalysts have been effectively determined using FTIR spectroscopy using the pyridine as a basic probe.

3.1.5. Temperature programme desorption of carbon dioxide (TPD-CO_2) analysis. TPD-CO_2 measurements were used to evaluate the basicity of the reduced catalysts. Fig. 6 displays CO_2 desorption profiles produced by the reduced catalysts during the TPD-CO_2 to determine the CO_2 adsorption
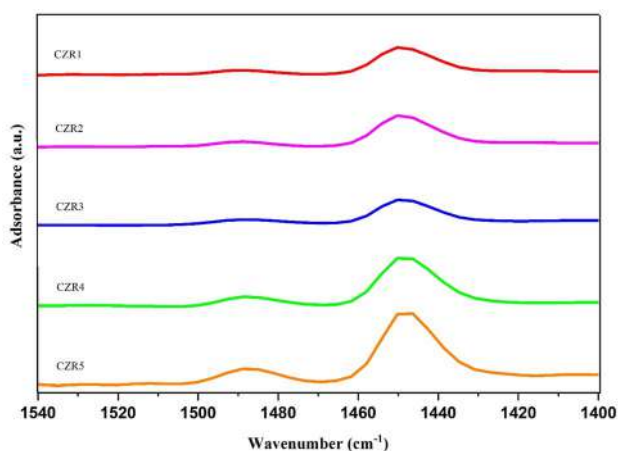

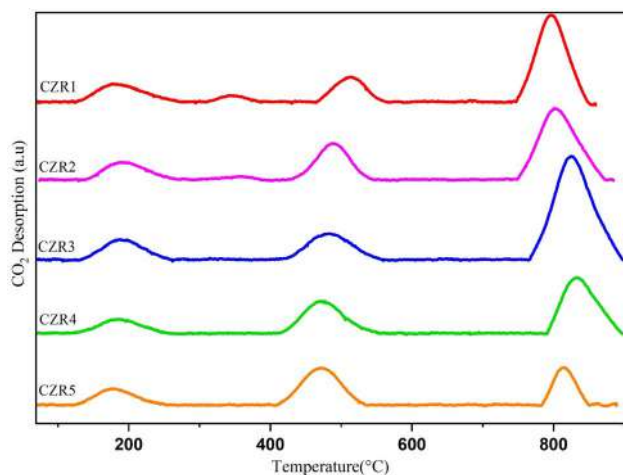Fig. 5 FTIR adsorbed pyridine of reduced catalysts.

Fig. 6 TPD-CO$_2$ analysis of reduced catalysts.

capabilities. Generally, the number of CO$_2$ species desorbed and the desorption temperature highlight the catalysts' surface-basic nature. There are three different types of basic sites for the RSBE-supported Cu/ZnO catalysts prepared in this work. In this way, CO$_2$ desorption below 300 °C, between 300 and 600 °C, and over 600 °C have each been linked to weak, moderate, and strong basic sites, respectively. Weak, moderate and strong basic sites correspond to surface hydroxyl (OH$^-$), metal–oxygen pair, and low coordination surface O^{2-}, respectively.[67] The catalytic performance of the related catalyst can be impacted by the adsorption ability of the catalysts for reactant CO$_2$ molecules. The adsorption is too weak or strong, which is not conducive to CO$_2$ activation or suppression in the chemical reaction.[68] For CO$_2$ reduction reactions, the amount of moderate surface basic sites with better capacities for adsorbing and activating highly-stable CO$_2$ molecules will determine CO$_2$ conversion. Additionally, moderate basic sites should allow the breakdown of intermediate species into the reaction products, enhancing RWGS reaction rates and reducing the carbonaceous species that block the active sites.[21]

The desorption profiles displayed by the reduced catalysts during the TPD-CO$_2$ studies suggested certain differences in the catalyst's basic properties. As seen in Fig. 6, a variation of the Cu/Zn ratio impacts the surface basicity of the catalysts. The intensity of the moderate basic site increased with the addition of the Cu/Zn ratio from 0.5 to 1.5, indicating that the increase in the Cu/Zn ratio can improve the adsorption performance of CO$_2$ molecules. In contrast, a further increase in Cu/Zn ratio showed an appreciable decrease in the intensity of moderate basic sites, which can weaken the adsorption or activation of CO$_2$. Wen et al. (2020) reported that adding Cu can prompt CO$_2$ adsorption and activation.[26] The increasing desorption amounts of CO$_2$ from moderate basic sites may be attributed to the electronic promotion effects of Cu dopant, more defect sites on the Cu–ZnO interface, providing additional active sites to adsorb CO$_2$.

Based on the finding, we may conclude that different Cu/Zn ratios create different basic sites. The beneficial effect of

increasing the Cu/Zn ratio to 1.5 could be attributed to the increase of the concentration of the surface's basic sites of moderate strength, which are believed to be responsible for catalyzing the C–O bond activation of adsorbed CO$_2$ species. It can be observed that the CZR3 catalyst exhibited the largest CO$_2$ desorption peak area among all the prepared catalysts, indicating its highest CO$_2$ adsorption capacity. The basicity of the tested samples increases as CZR5 < CZR4 < CZR1 < CZR2 < CZR3. TPD-CO$_2$ characterizations indicate that the catalyst's moderate Cu/Zn ratio in catalyst could modulate the acidity of the catalyst's surface, promoting RWGS reaction to CO.

3.1.6. Nitrogen physisorption isotherm analysis. N$_2$ physisorption isotherms were used to examine the textural properties of the reduced catalysts and RSBE support. As observed in Table 2, the BET surface area and total pore volume of the RSBE support is higher than both catalysts and possess a smaller pore size of 9.13 nm compared to the catalyst, indicating a mesoporous material. After copper and zinc impregnation on RSBE, the BET surface areas and total pore volume of all the catalysts decreased, whereas pore sizes increased. It indicates that Cu particles gathered around the pore mouths and partially clogged the supports' pores, and this should have resulted in a lower surface area and pore volume of the catalysts. Besides, the increases in pore size following the metal impregnation could be attributed to the incorporation of metal into the RSBE network, which causes the pore walls to contract and the pore diameter to expand.[21]

The BET surface area of the reduced catalysts increased in CZR1 < CZR3 < CZR2 < CZR4 < CZR5. The analysis of the BET surface area in the present study differs from the research of Álvarez Galván et al., who discovered that an increase in the Cu/Zn ratio causes a decrease in surface area due to the crystal grain development or particle aggregation.[24] However, Halim et al. found that increasing Cu loading of Cu/SiO$_2$ causes an initial increase in catalyst surface area, which might be
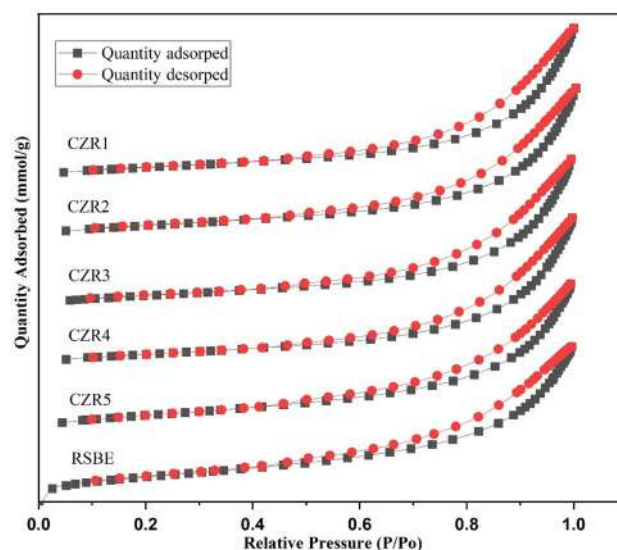

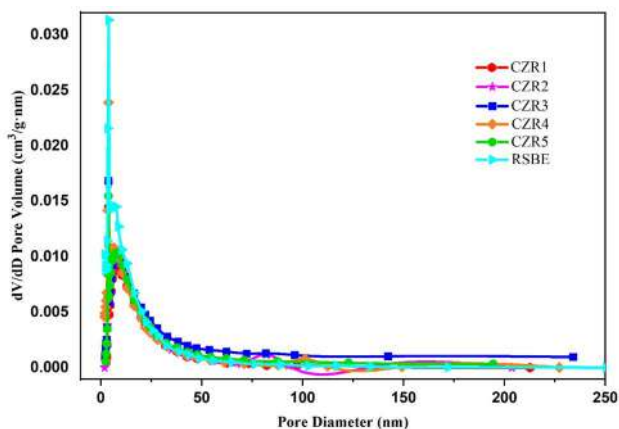**Fig. 7** N$_2$ adsorption–desorption isotherms of reduced catalysts and RSBE.

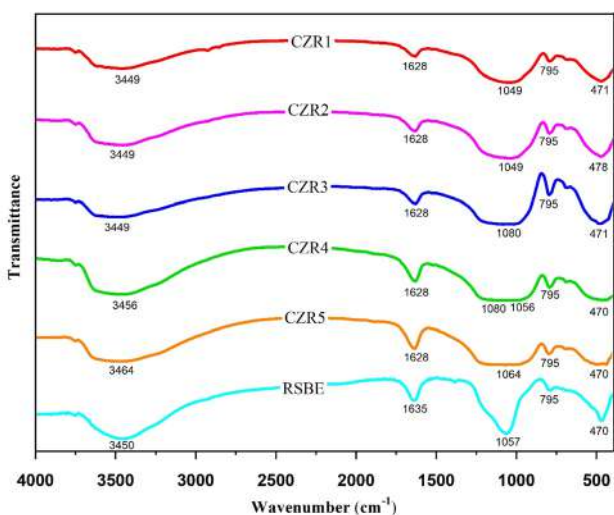Fig. 8 BJH pore size distribution of reduced catalysts.

Fig. 9 FTIR spectra of catalysts and RSBE support.

attributed to the phenomena of metal-assisted chemical etching, while the latter decrement in surface area is caused by the particle agglomeration.[69] Similar behaviour was observed by Zhang et al., who found that the BET surface area increased with increasing copper loading.[70] As mentioned by López et al., copper loading over the appropriate level does not boost catalytic activity.[71]

Fig. 7 and 8 show the N_2 adsorption–desorption isotherms and pore size distribution of reduced catalysts and RSBE. According to IUPAC, the isotherms for all the catalysts and RSBE support are categorized as type IV isotherms with a type H3 hysteresis loop, suggesting the presence of a mesoporous structure. The interparticle textural porosity is related to the capillary condensation seen at relatively high of the p/p_0 in the mesoporous structure of catalysts.[21,68] Variations in the relative pressure at which capillary condensation occurs indirectly relate to different particle sizes.[72] Concerning the RSBE support for which condensations were observed around 0.3 relative pressures, the higher relative pressures displayed by catalysts

($p/p_0 > 0.45$) suggest that Cu and Zn addition resulted in slightly smaller particle sizes. Almost similar condensation values were observed for all the catalysts. The BJH pore size distribution plots in Fig. 8 show that every sample are mesoporous materials (2–50 nm). It may be concluded from these findings that mesoporous structures can be effectively produced on all the catalysts. As a consequence, the Cu/Zn ratio had a substantial impact on the surface area of the produced catalysts, implying that the Cu-containing phase is mostly dispersed on the composite's surface.

3.1.7. FTIR analysis. The functional groups of the catalysts and the RSBE support are investigated using FTIR spectroscopy. The FTIR spectra of the catalysts and RSBE support within region 400–4000 cm^{-1} are displayed in Fig. 9. The spectra at 1049, 1056, 1057, 1064 and -1080 cm^{-1} are attributed to the silicate matrix's presence (Si–O–Si stretching vibrations). The presence of silica/quartz impurities (Si–O vibrations) is shown by the spectra at 795 cm^{-1}, while the spectra at 470, 471, and 478 cm^{-1} are attributed to the Si–O–Al vibrations.[46,73–75] The similar spectra of RSBE and catalyst exhibited suggest that the copper and zinc loading had no impact on the bleaching earth montmorillonite structure. This XRD analysis backed up this conclusion. The presence of interlayer water inside the catalysts is further confirmed by the adsorption band of the O–H stretching at bending vibrations of 1628 and 1635 cm^{-1}. In addition, the O–H vibration is also responsible for the broad adsorption peak at 3449, 3450, 3456 and 3464 cm^{-1} in the interlayer. The strength of the O–H group adsorption band diminishes after doping Cu and ZnO with RSBE, indicating that the O–H group adsorption band has decreased.[76] Cu and ZnO are substituted into the catalytic support, RSBE, according to the FTIR spectrum of catalysts. A similar trend was presented by Mestari et al., who found that the doping of Cu in the interlayer space of clay can be observed at the peaks attached to the water molecule.[77]

3.1.8. TEM analysis. The morphological properties of the CZR3 catalyst are shown in Fig. 10 after the investigation of TEM. Copper particles were detected as dark black, while zinc oxide was classified as light grey. A partial cross-link structure and a nanometer size of 27.8 nm for the CZR3 catalyst particles are revealed in the TEM image. The average particle sizes identified using TEM microscopy imply that the Cu crystal was nearly identical to that found using XRD. As a result, both techniques produced a very excellent agreement for the CZR3 catalyst. From Fig. 10(a), the TEM image and energy dispersive X-ray (EDX) element mapping of the CZR3 catalyst indicates that Cu and Zn particles are highly dispersed in different locations on the RSBE support. For high catalytic performance, they are advantageous features. However, the EDX detected the presence of oxides of silicon (Si), aluminium (Al), magnesium (Mg), iron (Fe), potassium (K), calcium (Ca) and titanium (Ti) in decreasing order of magnitude. These metal oxides are the composition of the RSBE. The Cu : Zn ratio was 3 : 2 based on the local elemental composition determined by TEM-EDX at several locations.
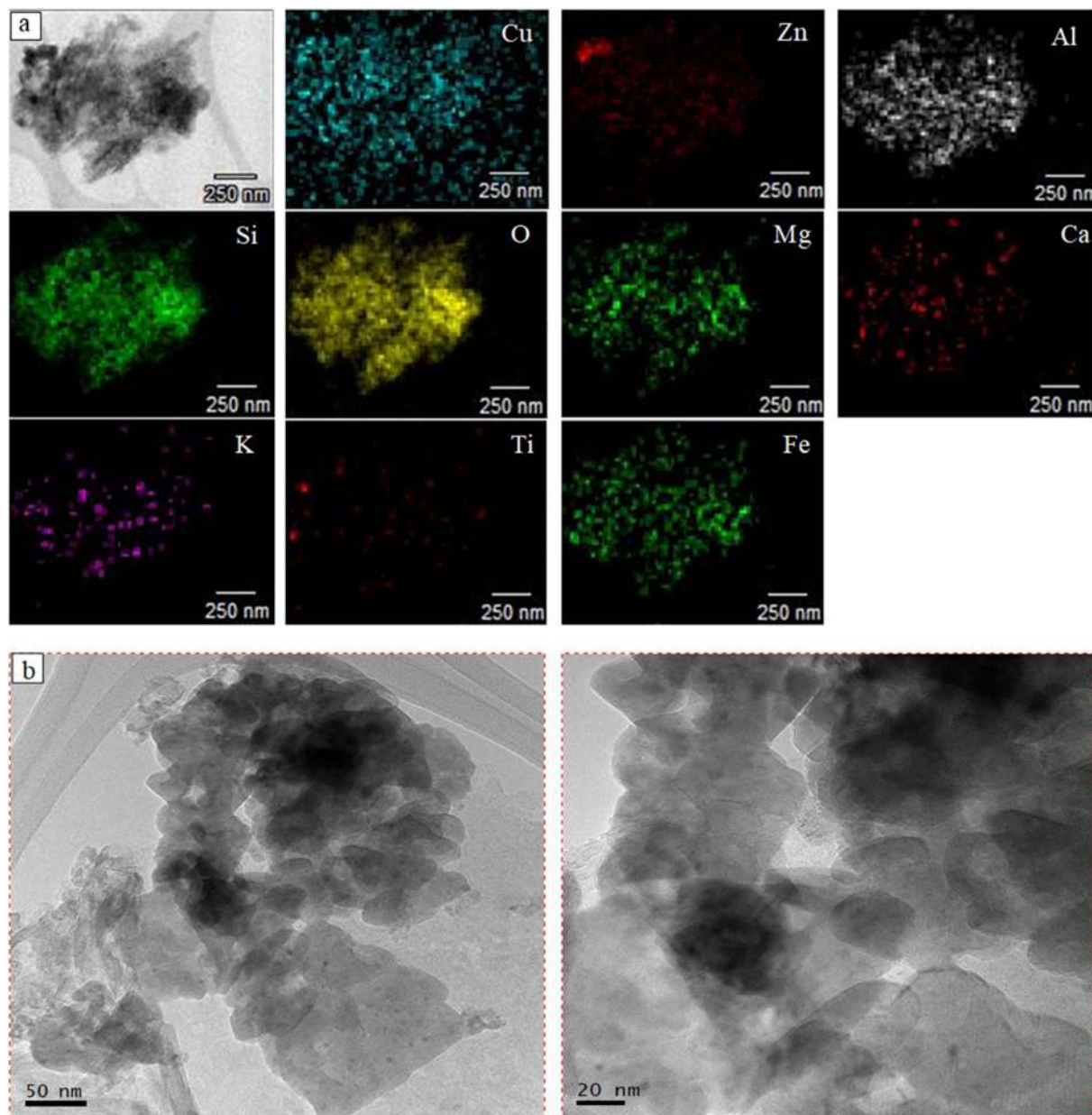
Fig. 10 TEM-EDX elemental mapping and HRTEM images for CZR3 catalyst: (a) TEM image and EDX mapping of CZR3 catalyst, and (b) HRTEM image of CZR3 catalyst.

3.2. Catalytic behaviour (catalyst screening)

The catalytic performance for the RWGS reaction of five different Cu/ZnO/RSBE catalyst types (CZR1, CZR2, CZR3, CZR4, and CZR5) produced from precursors with various Cu/Zn ratios (0.5, 1.0, 1.5, 2.0, 3.0) were assessed in a slurry reactor under the similar condition to identify the most promising catalyst. The catalytic activity was performed at 200 °C, 3 MPa, catalyst loading of 1.0 g, and an H_2/CO_2 ratio of 3. After 4 h of residence time, the experimental results were obtained. Fig. 10 reflects experimental results of various catalysts for RWGS reaction in terms of CO_2 conversion, CO yield, and H_2O yield. According to Fig. 10, the catalytic performance for converting CO_2 to CO is ranked in the order of CZR3 > CZR4 > CZR5 > CZR2 > CZR1. The

catalyst with a Cu/Zn ratio of 1.5 had a promotional effect on the catalyst's performance, which increased CO_2 conversion while maintaining a high CO yield. However, a minor amount of H_2O was produced, while no CH_4 was detected. Due to the active Cu sites, CO and H_2O are produced. CO_2 oxidizes Cu^0 to be C^+ and CO, while H_2 reduces Cu^+ to Cu^0 and produces H_2O.[78]

The results shown in Fig. 10 displayed that increasing the Cu/Zn ratio from 0.5 to 1.5 improved CO_2 conversion and CO yield up to 40.67 and 39.91%. Adding metallic Cu to the catalysts speeds up the reaction by increasing the number of active sites at the Cu/ZnO/RSBE catalytic interface, which has been hypothesized as the reaction's active species. As the Cu/Zn ratio increased over 1.5, the catalytic activity declined, decreasing

CO_2 conversion and CO yield to 33.24 and 28.21%. It might cause by the formation of larger Cu crystallites and less dispersed particles of the catalysts. Moreover, Zn presented in the catalyst is thought to influence CO_2 conversion and CO yield. The ideal Cu/ZnO interface on the RSBE catalyst support for CO_2 activation appears to be provided by an "activated ZnO" with an optimum Cu/Zn ratio.[24] The elemental ratios of Cu/Zn are correlated with the appearance of activation energy and activity trends.

In stark contrast, compared to other catalysts, CZR1 and CZR2 had poorer CO_2 conversion. As a result, CZR1 and CZR2 reduce the CO yield more than the other three catalysts. Interestingly, CZR1 and CZR2 performed less well than other catalysts, despite producing smaller copper crystallites and highly dispersed particles. The discrepancy shows that copper crystallite size and particle dispersion in the catalyst are not the only factors affecting the performance of Cu/ZnO/RSBE catalysts. Furthermore, CZR1 and CZR2 presented the weakest interactions between CuO and ZnO in catalysts shown by TPR-H_2 analysis. It has been postulated that the stronger metal support interactions in the catalyst could create unique electronic features at the interface to facilitate the CO2 transformation in RWGS reaction to produce CO and thereby benefit the reaction.[21] Additionally, a catalyst with a higher surface area increases the likelihood of collision between the reactants in contact with the surface of the catalyst, which enhances the RWGS reaction. However, CZR4 and CZR5 catalysts with higher surface areas and stronger metal support interactions do not perform as the most promising catalysts in CO_2 conversion and CO yield because they have larger Cu crystalline sizes and lower dispersion. Besides, the more significant pyridine adsorption sites shown at CZR4 and CZR5 would inhibit the CO_2 from being adsorbed or activated.

It also supports the existence of other characteristics that might influence the activity of the catalysts. In this regard, it is possible to note that the basicity of the catalysts also impacted their ability to perform. The RWGS reaction depends heavily on the surface basic sites. The higher basicity of the catalyst has been hypothesized to be advantageous for the adsorption or activation of the acidic gas CO_2, and further hydrogenation to CO. TPD-CO_2 analysis reveals that CZR3 exhibited the highest basicity among all the catalysts. Despite having a smaller surface area (66.76 m^2 g^{-1}), the CZR3 catalyst demonstrated the largest amount of CO_2 conversion, and CO yield among the catalysts studied. In addition, the XRD analysis shows that the CZR3 catalyst exhibited a small copper crystallite size (27.10 nm) and high metal dispersion (3.73%). It is high because the small Cu particles enhance catalytic performance by increasing the exposed surface area of the catalyst's active sites.

The joint presence of these properties may have caused the activity enhancement for the CZR3 catalyst. The inference is reasonable to explain CZR1 catalyst performed the least well of any of the catalysts, given that it had a limited surface area (59.56 m^2 g^{-1}) and weak interactions between metal oxide and support. Although the CZR5 catalyst had the strongest metal oxide support interaction, its activity may have been hindered by the large copper crystallite size in the catalyst (30.44 nm), which caused it to perform only moderately in the process.

A moderate Cu/Zn ratio of 1.5 in Cu/ZnO/RSBE catalyst can improve the ability of the catalyst surface to bind H_2 molecular and dissociated H species, resulting in enhanced CO production from the RWGS reaction. It is demonstrated that the physicochemical characteristics of catalysts were proven to impact the RWGS reaction. In contrast, selecting a catalyst's appropriate Cu/Zn ratio was more important. Recent investigations suggested that the surface basicity of the catalyst is crucial for catalytic selectivity.[21,26,29,79] Due to the intense competition with CO_2 methanation, which uses significantly more hydrogen and limits syngas generation, the product yield is vital to regulate this reaction and enhance conversion. In this regard, all the catalysts maintain only CO produce at 200 °C with no methane form.

The CO_2 conversion improves with increasing temperature, as anticipated by thermodynamic equilibrium and previously documented. However, this study proves that Cu/ZnO-based catalyst supported on RSBE can be worked at low temperatures with no methane and methanol form as the by-product. The products were CO and H_2O, with no methane detected in the study of Jurković et al. (2017), as expected for Cu-based catalysts.[35] In addition, the high surface area of RSBE was proved to act as promising support in the Cu/ZnO-based catalyst system with higher content of SiO_2, which is supported by the XRD analysis.

3.3. Optimizing process parameters to improve CO_2 conversion in the slurry concept

The CZR3 catalyst, which demonstrated the highest CO_2 conversion and CO production, was chosen for further investigation to determine the relationship between the different operating parameters on the catalytic performance of the RWGS reaction. The following experiment aimed to enhance further CO_2 conversion in the slurry reaction system, which uses light mineral oil as the carrier liquid. The effect of the reaction temperature (180–280 °C), pressure (1–5 MPa), reaction time (1–6 h), and catalyst weight (0.25–1.5 g) with an H_2 : CO_2 molar ratio of 3 was explicitly investigated for the RWGS reaction. It can be seen that the products are mainly CO followed by a minor amount of by-product, H_2O. If the water is removed from the end products, the CO_2 would have been completely reduced to CO, indicating that Cu/ZnO/RSBE catalyst is a promising RWGS catalyst under the present study.

3.3.1. Effect of temperature on improving CO_2 conversion. The reaction temperature significantly influences the CO_2 conversion to CO due to the complexity of the reaction scheme. Fig. 11 illustrates the effect of the reaction temperature (T = 180–280 °C) on the catalytic performance of the CZR3 catalyst at pressure = 3 MPa, reaction time = 4 h, and catalyst weight = 1.0 g.

The positive influence of increasing temperature on CO_2 conversion can be seen in Fig. 11. CZR3 catalyst demonstrated lower CO_2 conversion of 35.73% with a lower CO yield of 33.49% at a low temperature of 180 °C. At 280 °C, the CO_2 conversion
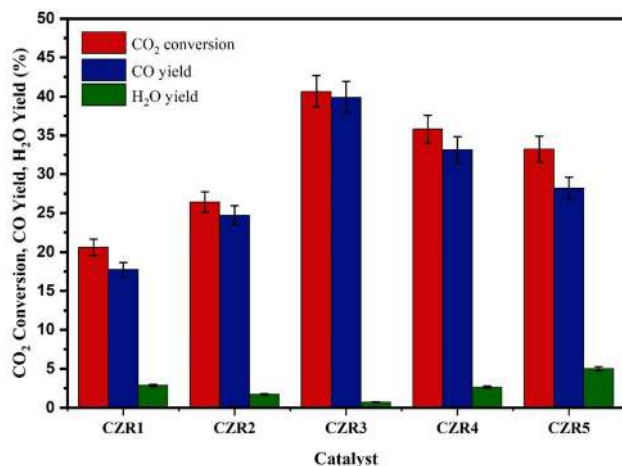
Fig. 11 The CO_2 conversion, CO yield, and H_2O yield in the reverse water gas shift reaction over various Cu/Zn ratios supported on RSBE. Catalytic reverse water gas shift reaction conditions: temperature = 200 °C; H_2/CO_2 = 3; pressure = 3 MPa; residence time = 4 h; catalyst weight = 1.0 g.

Fig. 12 Effect of reaction temperature on CO_2 conversion, CO yield and H_2O yield over CZR3 catalyst.

and CO yield reached 48.12% and 47.41%, respectively. It is clear that when the reaction temperature (180–280 °C) increased, CO_2 conversion and CO yield also increased. The findings concluded that the CO_2 conversion of the RWGS reaction increases with increasing temperature, which is consistent with earlier research.[23,27,29,35,80] Given that RWGS is an endothermic process, it makes sense that CO_2 conversion increases both kinetically and thermodynamically with rising temperatures, as seen in Fig. 11. Higher reaction temperatures are anticipated to boost CO_2 conversion to CO because the kinetic energy of the reactants will be adequate to accelerate the rate of mass transfer and overcome the diffusion resistance among the reactant gases (CO_2 and H_2), oil and catalyst. The H_2O yield decreased as the reaction temperature increased, which can be explained by the endothermic RWGS reaction. By increasing the reaction temperature, the thermodynamic equilibrium of the RWGS reaction is shifted to the CO product, which is higher than the by-product, H_2O, resulting in a high CO yield in the product stream.

The CO_2 conversion to CO significantly increases from 35.73 to 48.12% with the increase in temperatures. However, the most significant improvements are at lower temperatures, between 180 and 240 °C. A relatively slight increase was observed in the CO_2 conversion and CO yield when the reaction temperature increased from 240 to 280 °C. This can be concluded that the oxygen vacancy structure of the catalyst was going to destroy, and the catalyst was gradually decomposing when the reaction temperature exceeded the catalyst's decomposition temperature regarding the catalytic mechanism.[81] According to the research of Wei et al., the number of oxygen vacancies and the rate of CO_2 dissociation is the key factors limiting the catalytic activity.[81] As a result, at relatively low temperatures, RWGS processes are more suited for regulating oxygen vacancies. Thus, the findings suggest that the reaction temperature of 240 °C is the most
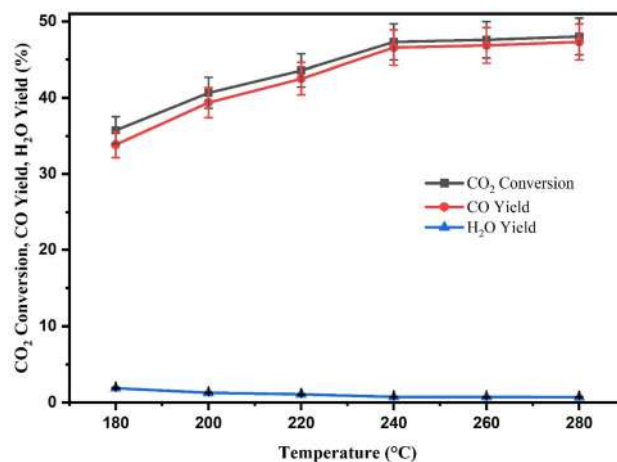
suitable for RWGS reaction using RSBE impregnated with Cu/ZnO catalyst.

3.3.2. Effect of pressure for improving CO_2 conversion. The effect of reaction pressure on the catalytic behaviour of the CZR3 catalyst was studied. Fig. 12 display variation of CO_2 conversion, CO yield and H_2O yield with reaction pressure ranging from 1–5 MPa, respectively, in the catalytic performance of the CZR3 catalyst at temperature = 240 °C, reaction time = 4 h, and catalyst weight = 1.0 g.

CO_2 conversion and CO yield increase with increasing reaction pressure, as shown in Fig. 12. The increased CO_2 conversion with pressure, which seems to disagree with the chemical equilibrium theory (pressure does not affect CO_2 conversion), can be interpreted by the following aspect. It is well known that gas absorption into the solvent is, within a specific range, proportional to the partial pressure of the gas. The concentration in the solvent increased as the gas pressure increased. So, the CO_2 conversion naturally increases when the reactant concentration also increases. Furthermore, certain catalysts have more challenging sites than others, such as those with small pores.[35] Thus, higher pressure would facilitate the penetration of the gas-phase molecules to these sites.

From thermodynamics, high pressure benefits methane and alcohol production from CO_2 hydrogenation. According to the RWGS study by Liu et al. (2017) as well as Li et al. (2013) over CuZnGaMO (M = Al, Zr) and Cu–Zn/K catalysts, product selectivity was strongly influenced by reaction pressure. The methanol yield and minor amount of CH_4 were observed in the high-pressure condition, which is in agreement with the methanation and methanol synthesis favour at higher reaction pressures due to the decrease in the number of gas moles.[29,82] However, no methane and alcohol are produced from the RWGS reaction in the present study. It can be seen that both CO_2 conversion and CO yield increased as the reaction pressure increased. Generally, the maximum CO_2 conversion of 46.78% was observed at a pressure of 5 MPa, but the most significant improvements are seen up to 3 MPa. The CO_2 conversion did not significantly

increase as the pressure was increased from 3 to 5 MPa. This might be attributed to the fact that the catalyst's surface is covered to a different extent at higher pressure conditions. This may eventually mean that variables such as the mean free path of surface diffusion may start to affect the reaction's kinetics.[35] Additionally, the pressure should have little to no impact on the reaction rate until a surface is virtually completely covered by the species.[35,83] From 3 MPa, the CZR3 catalyst demonstrates only <1% of performance in terms of CO_2 conversion and CO yield. As a result, the RWGS reaction using RSBE impregnated with Cu/ZnO catalyst was restricted to a maximum reaction pressure of 3 MPa.

3.3.3. Effect of reaction time for improving CO_2 conversion.

Fig. 13 describes the effect of reaction time on CO_2 conversion, CO yield, and H_2O yield. The experiment was conducted by varying the residence time from 1 to 6 h at $T = 240\ °C$, $P = 3$ MPa and catalyst loading = 1.0 g.

The results showed that when reaction time increased from 1 to 5 h, the CO_2 conversion and CO yield also increased. As a result, it can be seen that at a lower reaction time of 1 and 2 h, the CZR3 catalyst showed lower CO_2 conversion of 10.82 and 11.98% with lower CO yield of 10.51 and 11.61%. Subsequently, the CO_2 conversion and CO yield were 35.26% and 34.40% at a residence time of 3 h, and from 4 h to 5 h, the CO_2 conversion and CO yield increased slightly from 43.78 and 42.84% to 47.62 and 46.67%. Further increases in reaction time did not significantly increase CO_2 conversion and CO yield. The difficulty in mixing and dispersing the reactant onto the catalyst surface causes the RWGS reaction to occur slowly in the initial stages since the catalyst is immersed in the light mineral oil, forming a slurry phase reaction. At a reaction time of 5 h, the CO_2 conversion and CO yield reached a maximum value of 47.62% and 46.67%. Therefore, the reactant can cross the energy barrier in 5 h to convert the CO_2 to CO. As expected, when it is noticed an increase in the reaction time occurs, the CO_2 conversion immediately tends to increase as well, which is demonstrated in Fig. 13.
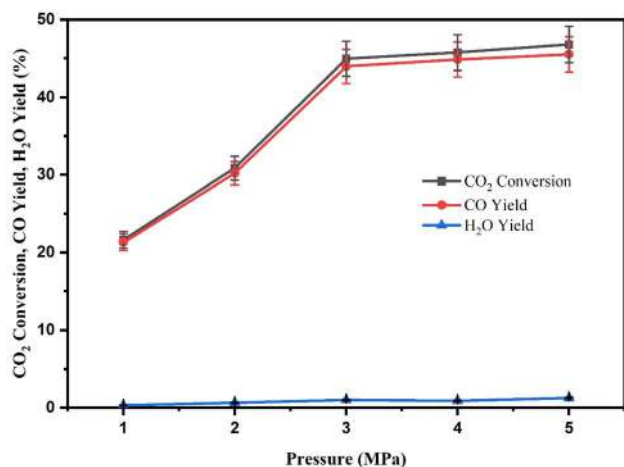

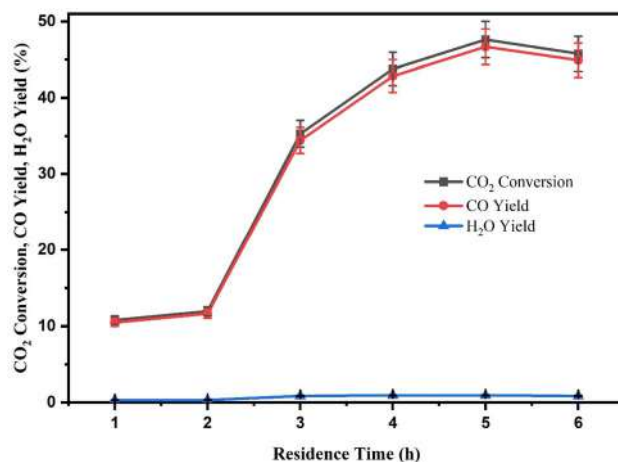**Fig. 13** Effect of reaction pressure on CO_2 conversion, CO yield and H_2O yield over CZR3 catalyst.

Fig. 14 Effect of residence time on CO_2 conversion, CO yield, and H_2O yield over CZR3 catalyst.

3.3.4. Effect of catalyst loading for improving CO_2 conversion.

Catalyst loading is essential in RWGS reaction to obtain optimum catalytic performance regarding CO_2 conversion and CO yield. In this study, the catalytic activities of the CZR3 catalyst were investigated with catalyst loading varying from 0.25 to 1.5 g at $T = 240\ °C$, $P = 3$ MPa, and reaction time = 5 h, and the results were presented in Fig. 14.

According to Fig. 14, increasing the catalyst loading from 0.25 to 1.25 g caused the CO_2 conversion and CO yield to increase from 15.92 and 15.64% to 48.76 and 45.14%, respectively. Increasing the amount of catalyst, the sufficient number of active sites present for the RWGS reaction in the slurry system causes the CO_2 conversion and CO yield to increase. The catalyst loading from 1.25 g to 1.5 g deteriorated CO_2 conversion and CO yield with decreases from 48.76 to 47.56% and 45.14 to 43.80%. An excessive amount of catalytic sites is expected to increase the reaction mixture's viscosity and cause poor diffusion of the reaction mixture, which decreases CO_2 conversion and CO yield. Hence, the rate becomes insensitive to further increases in catalyst loading. Additionally, higher catalyst loading may result in CO_2 absorption on the unused catalyst's surface, lowering CO_2 conversion and CO production. Even though by exceeding 1.0 g of catalyst loading, the CZR3 catalyst demonstrates almost the same CO_2 conversion and CO yield performance. Based on this result, the catalyst loading was limited to 1.0 g and was selected as the optimum catalyst loading for the RWGS reaction using RSBE impregnated with Cu/ZnO catalyst.

3.4. Recycling studies

CZR3 catalyst and the light mineral oil were recycled in five consecutive batch mode reactions at optimized temperature, pressure, reaction time and catalyst weight (240 °C, 3 MPa, 5 h and 1.25 g) to test the stability of the slurry CO generation system. The achieved CO_2 conversion, and CO yield for five consecutive runs are displayed in Fig. 15 to enable a technological evaluation of the slurry concept. The catalyst showed good stability throughout the process without significant CO_2
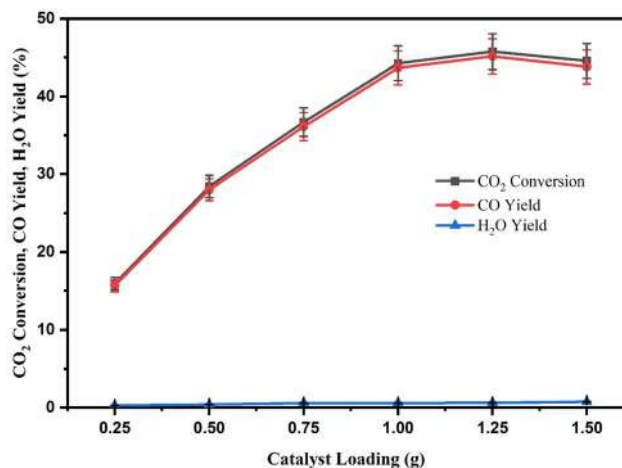
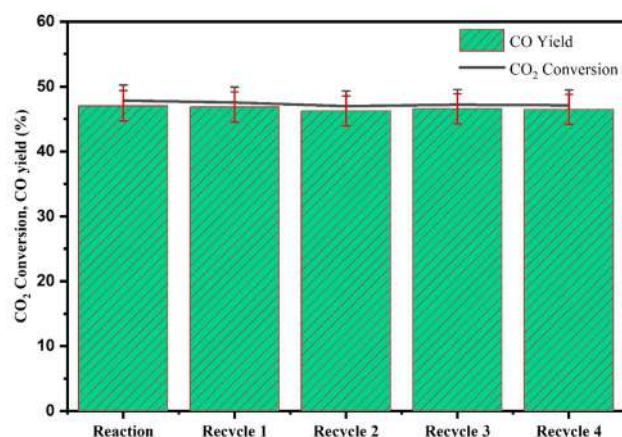Fig. 15 Effect of catalyst loading on CO_2 conversion, CO yield and H_2O yield over CZR3 catalyst.

Fig. 16 Catalyst stability test by recycling catalyst in batch mode experiments. CZR3 catalyst and light mineral oil were used five times under similar reaction conditions: temperature = 240 °C; pressure = 3 MPa; residence time = 5 h; catalyst weight = 1.25 g; H_2/CO_2 = 3.

conversion and CO yield loss. After 25 hours on stream, the result displayed in Fig. 15 demonstrates that CO_2 conversion and CO yield hold steady at around 47.32% and 46.64% for five successive cycles. Therefore, no significant decrease in CO_2 conversion and CO yield after recycling was observed. The outcome shows that this enhanced catalyst can continuously operate while providing a good activity/stability compromise. In terms of this aspect, the CZR3 catalyst may be one promising candidate for industrial application. Hence, reaction performance was unaffected in recycling tests with a 25 h total reaction duration (Fig. 16).

4. Conclusions

This research produced a series of highly active Cu/ZnO-based catalysts supported on the RSBE (CZR1, CZR2, CZR3, CZR4, and CZR5) for the RWGS reaction. All of the samples are active, with a strong preference for CO. Among the catalysts in the

present study, the CZR3 catalyst with a Cu/Zn ratio of 1.5 was the most promising catalyst. At operating conditions of 200 °C, 3 MPa, catalyst loading of 1.0 g, and reaction time of 4 h, CZR3 presented a maximum CO yield of 39.91%. The CO_2 conversion and CO selectivity attained by CZR3 were 40.67% and 98.13%, respectively. The outstanding performance of CZR3 is strongly correlated with the coexistence of high surface basicity, which makes it simpler to adsorb/activate the acidic gas CO_2, resulting in higher CO_2 conversion and CO production.

On the other hand, the conversion of CO_2 strongly depends on the reaction temperature, pressure, reaction time, and catalyst loading. The RWGS reaction carried out at 240 °C, 3 MPa, 5 h with 1.25 g catalyst loading over CZR3 catalyst enhances the catalytic performance by achieving 48.76% CO_2 conversion and approaches 45.14% CO yield. Also, it has been demonstrated that the CZR3 catalyst can be recycled successfully for five consecutive runs without a discernible drop in CO_2 conversion and CO yields. Indeed, the Cu/ZnO catalyst supported on RSBE is a selective catalyst for RWGS reaction and facilitates CO_2 adsorption on the catalyst surface at lower temperatures with less demand of conversion unit, which suppresses the generation of the low value-added side-product such as methane. In conclusion, the studies that have been presented show promise for the RWGS reaction in slurry reactors using Cu/ZnO/RSBE catalysts. Overall, the significant CO_2 conversion for CO production achieved with the innovative Cu/ZnO/RSBE catalysts points to the effective design of our engineered catalytic materials and suggests that it is suitable for practical applications in gas-phase chemical CO_2 recycling.

Author contributions

M. L. P. Phey: first author, contents development and writing. T. A. Tuan Abdullah: supervision, methodology, writing and funding. U. F. M. Ali: writing and editing. M. Y. Mohamud: writing, experiment and methodology. M. Ikram: english revision and conceptualization. W. Nabgan: proofreading and english editing.

Conflicts of interest

The authors declare that they have no known competing financial interests or personal relationships that could have appeared to influence the work reported in this paper.

Acknowledgements

References

1 J. Blunden and T. Boyer, State of the climate in 2020, *Bull. Am. Meteorol. Soc.*, 2021, **102**(8), 1–481.

2 B. Metz, O. Davidson and P. Bosch, Climate Change 2007 University of Sierra Leone, *Waste Manag.*, 2007, https://www.cambridge.org/es/academic/subjects/earth-and-environmental-science/climatology-and-climate-change/climate-change-2007-physical-science-basis-working-group-i-contribution-fourth-assessment-report-ipcc?format=PB&isbn=9780521705967.

3 H. Abdul Rahman, Global climate change and its effects on human habitat and environment in Malaysia, *Mal. J. Environ. Manag.*, 2011, **10**(2), 17–32.

4 H. Zhong, *et al.*, Synergistic electroreduction of carbon dioxide to carbon monoxide on bimetallic layered conjugated metal–organic frameworks, *Nat. Commun.*, 2020, **11**(1), 1–10.

5 J. Gao, *et al.*, Highly Selective and Efficient Electroreduction of Carbon Dioxide to Carbon Monoxide with Phosphate Silver-Derived Coral-like Silver, *ACS Sustainable Chem. Eng.*, 2019, **7**(3), 3536–3543.

6 F. Y. Gao, R. C. Bao, M. R. Gao and S. H. Yu, Electrochemical CO_2-to-CO conversion: electrocatalysts, electrolytes, and electrolyzers, *J. Mater. Chem. A*, 2020, **8**(31), 15458–15478.

7 J. L. Grant, K. Goswami, L. O. Spreer, J. W. Otvos and M. Calvin, Photochemical Reduction of Carbon Dioxide to Carbon Monoxide in Water using a Nickel(II) Tetra-azamacrocycle Complex as Catalyst, *J. Chem. Soc. Dalton Trans.*, 1987, 2105–2109.

8 J. Ettedgui, Y. Diskin-Posner, L. Weiner and R. Neumann, Photoreduction of carbon dioxide to carbon monoxide with hydrogen catalyzed by a rhenium(I) phenanthroline–polyoxometalate hybrid complex, *J. Am. Chem. Soc.*, 2011, **133**(2), 188–190.

9 T. A. Kistler, M. Y. Um, J. K. Cooper, I. D. Sharp and P. Agbo, Monolithic Photoelectrochemical CO_2 Reduction Producing Syngas at 10% Efficiency, *Adv. Energy Mater.*, 2021, **11**(21), 1–29.

10 Q. Zhai, *et al.*, Photocatalytic conversion of carbon dioxide with water into methane: platinum and copper(I) oxide co-catalysts with a core–shell structure, *Angew. Chem., Int. Ed.*, 2013, **52**(22), 5776–5779.

11 H. Zhou, J. Guo, P. Li, T. Fan, D. Zhang and J. Ye, Leaf-architectured 3D hierarchical artificial photosynthetic system of perovskite titanates towards CO_2 photoreduction into hydrocarbon fuels, *Sci. Rep.*, 2013, **3**, 1–9.

12 L. Gustavsson, P. Börjesson, B. Johansson and P. Svenningsson, Reducing CO_2 emissions by substituting biomass for fossil fuels, *Energy*, 1995, **20**(11), 1097–1113.

13 F. Gabriel Acien Fernandez, C. V. González-López, J. M. Fernández Sevilla and E. Molina Grima, Conversion of CO_2 into biomass by microalgae: How realistic a contribution may it be to significant CO_2 removal?, *Appl. Microbiol. Biotechnol.*, 2012, **96**(3), 577–586.

14 S. Roy, *et al.*, High-Flux Solar-Driven Thermochemical Dissociation of CO_2 and H_2O Using Nonstoichiometric Ceria, *Science*, 2010, **330**(6012), 1797–1801.

15 P. Furler, J. Sche, M. Gorbar, L. Moes, U. Vogt and A. Steinfeld, Solar Thermochemical CO_2 Splitting Utilizing a Reticulated Porous Ceria Redox System, *Energy Fuels*, 2012, **26**(11), 7051–7059.

16 A. Le Gal, S. Abanades and G. Flamant, Thermochemical CO_2 and CO_2/H_2O Splitting over $NiFe_2O_4$ for Solar Fuels Synthesis, *Energy Fuel.*, 2011, **25**, 4836–4845.

17 A. H. McDaniel, *et al.*, Sr- and Mn-doped $LaAlO_{3-\delta}$ for solar thermochemical H_2 and CO production, *Energy Environ. Sci.*, 2013, **6**(8), 2424–2428.

18 A. H. Bork, M. Kubicek, M. Struzik and J. L. M. Rupp, Perovskite $La_{0.6}Sr_{0.4}Cr_{1-x}Co_xO_{3-\delta}$ solid solutions for solar-thermochemical fuel production: strategies to lower the operation temperature, *J. Mater. Chem. A*, 2015, **3**(30), 15546–15557.

19 F. G. Becker, *et al.*, CO_2 conversion by reverse water gas shift catalysis: comparison of catalysts, mechanisms and their consequences for CO_2 conversion to liquid fuels, *Syria Stud.*, 2015, **7**(1), 37–72.

20 A. Okemoto, M. R. Harada, T. Ishizaka, N. Hiyoshi and K. Sato, Catalytic performance of MoO_3/FAU zeolite catalysts modified by Cu for reverse water gas shift reaction, *Appl. Catal., A*, 2020, **592**, 117415.

21 M. González-Castano, J. C. Navarro De Miguel, F. Sinha, S. Ghomsi Wabo, O. Klepel and H. Arellano-Garcia, Cu supported $Fe–SiO_2$ nanocomposites for reverse water gas shift reaction, *J. CO2 Util.*, 2021, **46**, 101493.

22 F. S. Stone and D. Waller, Cu–ZnO and $Cu–ZnO/Al_2O_3$ catalysts for the reverse water–gas shift reaction. The effect of the Cu/Zn ratio on precursor characteristics and on the activity of the derived catalysts, *Top. Catal.*, 2003, **22**(3–4), 305–318.

23 L. Pastor-Pérez, F. Baibars, E. Le Sache, H. Arellano-García, S. Gu and T. R. Reina, CO_2 valorization *via* reverse water–gas shift reaction using advanced Cs doped $Fe–Cu/Al_2O_3$ catalysts, *J. CO2 Util.*, 2017, **21**, 423–428.

24 C. Álvarez Galván, J. Schumann, M. Behrens, J. L. G. Fierro, R. Schlögl and E. Frei, Reverse water–gas shift reaction at the Cu/ZnO interface: influence of the Cu/Zn ratio on structure–activity correlations, *Appl. Catal., B*, 2016, **195**, 104–111.

25 L. Zhang, Q. Song, Y. Xing, Z. Si, Y. Liu, R. Ran, X. Wu, D. Weng, and F. Kang, Active and Stable $MgAl_2O_4$ and $Ni(SA)/MgAl_2O_4$ Catalys for the Reverse Water Gas Shift Reaction, 2021, 2021050562, Preprints, DOI: 10.20944/preprints202105.0562.v1.

26 J. Wen, *et al.*, The study of reverse water gas shift reaction activity over different interfaces: the design of Cu-plate ZnO model catalysts, *Catalysts*, 2020, **10**(5), 533.

27 L. Pastor-Pérez, M. Shah, E. Le Saché and T. R. Reina, Improving Fe/Al_2O_3 catalysts for the reverse water–gas shift reaction: on the effect of cs as activity/selectivity promoter, *Catalysts*, 2018, **8**(12), 608.

28 Y. Shen, Z. Cao and Z. Xiao, An efficient support-free nanoporous Co catalyst for reverse water–gas shift reaction, *Catalysts*, 2019, **9**(5), 423.

29 X. Liu, P. Ramírez de la Piscina, J. Toyir and N. Homs, CO_2 reduction over Cu–ZnGaMO (M = Al, Zr) catalysts prepared by a sol–gel method: unique performance for the RWGS reaction, *Catal. Today*, 2017, **296**, 181–186.

30 M. Zhu, Q. Ge and X. Zhu, Catalytic Reduction of CO_2 to CO via Reverse Water Gas Shift Reaction: Recent Advances in the Design of Active and Selective Supported Metal Catalysts, *Trans. Tianjin Univ.*, 2020, **26**(3), 172–187.

31 R. M. Bown, M. Joyce, Q. Zhang, T. R. Reina and M. S. Duyar, Identifying Commercial Opportunities for the Reverse Water Gas Shift Reaction, *Energy Technol.*, 2021, **9**(11), 28–31.

32 M. González-Castaño, B. Dorneanu and H. Arellano-García, The reverse water gas shift reaction: a process systems engineering perspective, *React. Chem. Eng.*, 2021, **6**(6), 954–976.

33 S. I. Fujita, M. Usui and N. Takezawa, Mechanism of the reverse water gas shift reaction over Cu/ZnO catalyst, *J. Catal.*, 1992, **134**(1), 220–225.

34 C. S. Chen, W. H. Cheng and S. S. Lin, Mechanism of CO formation in reverse water–gas shift reaction over Cu/Al_2O_3 catalyst, *Catal. Lett.*, 2000, **68**(1–2), 45–48.

35 D. L. Jurković, A. Pohar, V. D. B. C. Dasireddy and B. Likozar, Effect of Copper-based Catalyst Support on Reverse Water–Gas Shift Reaction (RWGS) Activity for CO_2 Reduction, *Chem. Eng. Technol.*, 2017, **40**(5), 973–980.

36 S. Natesakhawat, P. R. Ohodnicki, B. H. Howard, J. W. Lekse, J. P. Baltrus and C. Matranga, Adsorption and deactivation characteristics of Cu/ZnO-based catalysts for methanol synthesis from carbon dioxide, *Top. Catal.*, 2013, **56**(18–20), 1752–1763.

37 Y. Wang, D. Yang, S. Li, L. Zhang, G. Zheng and L. Guo, Layered copper manganese oxide for the efficient catalytic CO and VOCs oxidation, *Chem. Eng. J.*, 2019, **357**, 258–268.

38 M. V Twigg and M. S. Spencer, Deactivation of Copper Metal Catalysts for Methanol Decomposition, Methanol Steam Reforming and Methanol Synthesis, *Top. Catal.*, 2003, **22**(3), 191–203.

39 K. Y. Cheong, S. K. Loh and J. Salimon, Effect of spent bleaching earth based bio organic fertilizer on growth, yield and quality of eggplants under field condition, *AIP Conf. Proc.*, 2013, **1571**, 744–748.

40 S. K. Loh and S. F. Cheng, A Study of Residual Oils Recovered from Spent Bleaching Earth: Their Characteristics and Applications, *Am. J. Appl. Sci.*, 2006, **3**(10), 2063–2067.

41 F. Marrakchi, M. Bouaziz and B. H. Hameed, Activated carbon–clay composite as an effective adsorbent from the spent bleaching sorbent of olive pomace oil: Process optimization and adsorption of acid blue 29 and methylene blue, *Chem. Eng. Res. Des.*, 2017, **128**, 221–230.

42 S. Suhartini, N. Hidayat and S. Wijaya, Physical properties characterization of fuel briquette made from spent bleaching earth, *Biomass Bioenergy*, 2011, **35**(10), 4209–4214.

43 S. K. Loh, K. Y. Cheong, Y. M. Choo and J. Salimon, Formulation and optimization of spent bleaching earth-based bio organic fertilizer, *J. Oil Palm Res.*, 2015, **27**(1), 57–66.

44 P. M. K. Prajitha and P. Pushpaletha, Catalyst Preparation, Characterization and Catalytic Activity of Kaolinite Clay from Nileswar, Kerala, *Int. J. Appl. Chem.*, 2017, **13**(3), 461–475.

45 P. L. Boey, M. I. Saleh, N. Sapawe, S. Ganesan, G. P. Maniam and D. M. H. Ali, Pyrolysis of residual palm oil in spent bleaching clay by modified tubular furnace and analysis of the products by GC-MS, *J. Anal. Appl. Pyrolysis*, 2011, **91**(1), 199–204.

46 W. T. Tsai, H. P. Chen, M. F. Hsieh, H. F. Sun and S. F. Chien, Regeneration of spent bleaching earth by pyrolysis in a rotary furnace, *J. Anal. Appl. Pyrolysis*, 2002, **63**(1), 157–170.

47 C. Su, L. Duan, F. Donat and E. J. Anthony, From waste to high value utilization of spent bleaching clay in synthesizing high-performance calcium-based sorbent for CO_2 capture, *Appl. Energy*, 2018, **210**, 117–126.

48 R. Macasil, A. P. Redublo, A. Santos, C. I. Torres and D. Pangayao, Geopolymerization of Coal Fly Ash, Ceramic Tile Waste and Spent Bleaching Earth for the Production of Sodium Aluminosilicate Monolith, *MATEC Web Conf.*, 2021, **333**, 12001.

49 T. Li, C. Fu, J. Qi, J. Pan, S. Chen and J. Lin, Effect of zinc incorporation manner on a $Cu–ZnO/Al_2O_3$ glycerol hydrogenation catalyst, *React. Kinet., Mech. Catal.*, 2013, **109**(1), 117–131.

50 M. G. Martinez, D. P. Minh, E. W. Hortala, A. Nzihou and P. Sharrock, Synthesis, characterization, and thermo-mechanical properties of copper-loaded apatitic calcium phosphates, *Compos. Interfaces*, 2013, **20**(8), 647–660.

51 C. Wisetrinthong, S. Pinitsoontorn, P. Kidkhunthod and K. Wongsaprom, Thermal decomposition synthesis and magnetic properties of crystalline zinc oxide powders, *J. Phys.: Conf. Ser.*, 2018, **1144**(1), 012078.

52 P. Kowalik and W. Próchniak, The effect of calcination temperature on properties and activity, *Ann. UMCS, Chem.*, 2010, **65**, 79–87.

53 X. Zhang, L. Zhong, Q. Guo, H. Fan, H. Zheng and K. Xie, Influence of the calcination on the activity and stability of the $Cu/ZnO/Al_2O_3$ catalyst in liquid phase methanol synthesis, *Fuel*, 2010, **89**(7), 1348–1352.

54 X. Guo, D. Mao, G. Lu, S. Wang and G. Wu, CO_2 hydrogenation to methanol over $Cu/ZnO/ZrO_2$ catalysts prepared via a route of solid-state reaction, *Catal. Commun.*, 2011, **12**(12), 1095–1098.

55 M. Behrens and R. Schlögl, How to prepare a good Cu/ZnO catalyst or the role of solid state chemistry for the synthesis of nanostructured catalysts, *Z. Anorg. Allg. Chem.*, 2013, **639**(15), 2683–2695.

56 S. F. H. Tasfy, N. A. M. Zabidi, M. S. Shaharun, D. Subbarao and A. Elbagir, Carbon dioxide hydrogenation to methanol over Cu/ZnO-SBA-15 catalyst: effect of metal loading, *Defect Diffus. Forum*, 2017, **380**, 151–160.

57 V. V. Thyssen, T. A. Maia and E. M. Assaf, Cu and Ni catalysts supported on γ-Al_2O_3 and SiO_2 assessed in glycerol steam reforming reaction, *J. Braz. Chem. Soc.*, 2015, **26**(1), 22–31.

58 A. V. Fedorov, R. G. Kukushkin, P. M. Yeletsky, O. A. Bulavchenko, Y. A. Chesalov and V. A. Yakovlev, Temperature-programmed reduction of model CuO, NiO and mixed CuO–NiO catalysts with hydrogen, *J. Alloys Compd.*, 2020, **844**, 156135.

59 C. I. Ezeh, X. Yang, J. He, C. Snape and X. M. Cheng, Correlating ultrasonic impulse and addition of ZnO promoter with CO_2 conversion and methanol selectivity of CuO/ZrO_2 catalysts, *Ultrason. Sonochem.*, 2018, **42**, 48–56.

60 S. Gesmanee, Catalytic hydrogenation of CO production in fixed-bed 2 for methanol assessing the feasibility of using the heat demand-outdoor temperature function for a long-term district heat demand forecast, *Energy Procedia*, 2017, **138**, 739–744.

61 X. Guo, D. Mao, S. Wang, G. Wu and G. Lu, Combustion synthesis of $CuO–ZnO–ZrO_2$ catalysts for the hydrogenation of carbon dioxide to methanol, *Catal. Commun.*, 2009, **10**(13), 1661–1664.

62 Y. Zhang, J. Fei, Y. Yu and X. Zheng, Methanol synthesis from CO_2 hydrogenation over Cu based catalyst supported on zirconia modified γ-Al_2O_3, *Energy Convers. Manage.*, 2006, **47**(18–19), 3360–3367.

63 G. Avgouropoulos, T. Ioannides and H. Matralis, Influence of the preparation method on the performance of $CuO–CeO_2$ catalysts for the selective oxidation of CO, *Appl. Catal., B*, 2005, **56**(1–2), 87–93.

64 H. Tian, Hydrogenation of biomass derivatives over Ni/clay catalyst: significant impacts of the treatment of clay with NaOH on the reaction network, *J. Chem. Technol. Biotechnol.*, 2021, **96**(9), 2569–2578.

65 S. Ren, *et al.*, Highly active and selective Cu–ZnO based catalyst for methanol and dimethyl ether synthesis via CO_2 hydrogenation, *Fuel*, 2019, **239**, 1125–1133.

66 C. Huang, S. Chen, X. Fei, D. Liu and Y. Zhang, Catalytic Hydrogenation of CO_2 to Methanol: Study of Synergistic Effect on Adsorption Properties of CO_2 and H_2 in $CuO/ZnO/ZrO_2$ System, *Catalysts*, 2015, **5**(4), 1846–1861.

67 P. Gao, *et al.*, Fluorinated Cu/Zn/Al/Zr hydrotalcites derived nanocatalysts for CO_2 hydrogenation to methanol, *J. CO2 Util.*, 2016, **16**, 32–41.

68 B. Dai, *et al.*, CO_2 reverse water–gas shift reaction on mesoporous M-CeO_2 catalysts, *Can. J. Chem. Eng.*, 2017, **95**(4), 634–642.

69 M. Y. A. Halim, W. L. Tan, N. H. H. Abu Bakar and M. A. Bakar, Surface characteristics and catalytic activity of copper deposited porous silicon powder, *Materials*, 2014, **7**(12), 7737–7751.

70 B. Zhang, S. Hui, S. Zhang, Y. Ji, W. Li and D. Fang, Effect of copper loading on texture, structure and catalytic performance of Cu/SiO_2 catalyst for hydrogenation of dimethyl oxalate to ethylene glycol, *J. Nat. Gas Chem.*, 2012, **21**(5), 563–570.

71 F. E. López-Suárez, A. Bueno-López and M. J. Illán-Gómez, Cu/Al_2O_3 catalysts for soot oxidation: copper loading effect, *Appl. Catal., B*, 2008, **84**(3–4), 651–658.

72 G. Leofanti, M. Padovan, G. Tozzola and B. Venturelli, Surface area and pore texture of catalysts, *Catal. Today*, 1998, **41**(1–3), 207–219.

73 M. R. Sabour and M. Shahi, Spent Bleaching Earth Recovery of Used Motor-Oil Refinery, *Civ. Eng. J.*, 2018, **4**(3), 572.

74 X. Liang, C. Yang, X. Su and X. Xue, Regeneration of spent bleaching clay by ultrasonic irradiation and their application in methylene blue adsorption, *Clay Minerals*, 2020, **55**(1), 24–30.

75 M. L. P. Phey, T. A. T. Abdullah, A. Ahmad and U. F. M. Ali, Application of regenerated spent bleaching earth as an adsorbent for the carbon dioxide adsorption by gravimetric sorption system, *J. Phys.: Conf. Ser.*, 2022, **2259**(1), 012015.

76 I. Ben Elkamel, N. Hamdaoui, A. Mezni, R. Ajjel and L. Beji, Synthesis and characterization of Cu doped ZnO nanoparticles for stable and fast response UV photodetector at low noise current, *J. Mater. Sci.: Mater. Electron.*, 2019, **30**(10), 9444–9454.

77 A. Mestari, *et al.*, Cu-bentonite as an efficient and recyclable material catalyst for the synthesis of benzimidazoles, benzoxazoles and benzothiazoles, *J. Mater. Environ. Sci.*, 2017, **8**, 4816–4823.

78 X. Su, X. Yang, B. Zhao and Y. Huang, Designing of highly selective and high-temperature endurable RWGS heterogeneous catalysts: recent advances and the future directions, *J. Energy Chem.*, 2017, **26**(5), 854–867.

79 L. X. Zhang, Y. C. Zhang and S. Y. Chen, Effect of promoter TiO_2 on the performance of $CuO–ZnO–Al_2O_3$ catalyst for CO_2 catalytic hydrogenation to methanol, *Ranliao Huaxue Xuebao*, 2011, **39**(12), 912–917.

80 F. Vidal Vázquez, P. Pfeifer, J. Lehtonen, P. Piermartini, P. Simell and V. Alopaeus, Catalyst Screening and Kinetic Modeling for CO Production by High Pressure and Temperature Reverse Water Gas Shift for Fischer–Tropsch Applications, *Ind. Eng. Chem. Res.*, 2017, **56**(45), 13262–13272.

81 Q. Wei, Z. Kai, Z. Na, Z. Lei, Q. Shao and G. A. O. Zhi, Enhanced $CuAl_2O_4$ Catalytic Activity via Alkalinization Treatment toward High CO_2 Conversion during Reverse Water Gas Shift Reaction, *Catalysts*, 2020, **12**(12), 1511.

82 S. G. Li, *et al.*, The reverse water–gas shift reaction and the synthesis of mixed alcohols over K/Cu–Zn catalyst from CO_2 hydrogenation, *Adv. Mater. Res.*, 2013, **772**, 275–280.

83 A. S. Malik, S. F. Zaman, A. A. Al-Zahrani, M. A. Daous, H. Driss and L. A. Petrov, Development of highly selective $PdZn/CeO_2$ and Ca-doped $PdZn/CeO_2$ catalysts for methanol synthesis from CO_2 hydrogenation, *Appl. Catal., A*, 2018, **560**, 42–53.